# Self-assembling biomaterials: Liquid crystal phases of cholesteryl oligo(L-lactic acid) and their interactions with cells

**Julia J. Hwang, Subramani N. Iyer, Li-Sheng Li, Randal Claussen, Daniel A. Harrington, and Samuel I. Stupp†**

Department of Materials Science and Engineering, Department of Chemistry, Feinberg School of Medicine, Northwestern University, Evanston, IL 60208

Edited by Robert Langer, Massachusetts Institute of Technology, Cambridge, MA, and approved May 2, 2002 (received for review December 13, 2001)

**We report here on the synthesis and characterization of a series of self-assembling biomaterials with molecular features designed to interact with cells and scaffolds for tissue regeneration. The molecules of these materials contain cholesteryl moieties, which have universal affinity for cell membranes, and short chains of lactic acid, a common component of biodegradable tissue engineering matrices. The materials were synthesized in good yields with low polydispersities in the range of 1.05–1.15, and their characterization was carried out by small-angle x-ray diffraction, transmission electron microscopy, electron diffraction, differential scanning calorimetry, and atomic force microscopy. These molecular materials form layered structures that can be described as smectic phases and can also order into single-crystal stacks with an orthorhombic unit cell. Their layer spacings range from 58 to 99 Å, corresponding to bilayers of oligomers with an average of 10 and 37 lactic acid residues, respectively. The self-organized layered structures were found to promote improved fibroblast adhesion and spreading, although the specific mechanism for this observed response remains unknown. The ability of self-assembling materials to present ordered and periodic bulk structures to cells could be a useful strategy in tissue engineering.**

Self-assembly strategies could bring novel capabilities to biomaterials used in advanced medicine and biotechnology. In a self-assembly strategy, a specific thermodynamically stable structure is targeted by design of specific molecules. The past decade has seen a great deal of progress in such strategies, including contributions from our laboratory (1–3). Self assembly of biomaterials would be particularly useful in medicine, because the formation of targeted structures could be programmed to occur on contact with tissues. Additionally, the control of three-dimensional structure can target the spatial presentation of bioactive ligands to impact directly the behavior of cells. Such control could impact a material's ability to promote cell division, differentiation, and synthesis of extracellular matrix. Self-assembling biomaterials could also be used to design with greater precision molecular delivery to cells. In this paper, we report on the design and synthesis of a novel family of self-assembling biocompatible structures by using cholesterol as a mesogen, intended to initiate the investigation of this general class of biomaterials.

The molecules of the model system studied here contain cholesterol moieties and short chains of oligo-(L-lactic acid) connected through an ester bond. Kricheldorf and Kreiser-Saunders (4) prepared by a similar methodology a series of poly(L-lactic acid) (PLA) molecules, end-functionalized with various vitamins, hormones, and drugs. Cholesterol moieties were selected in the molecular design of our system for several reasons. One is the thermodynamic affinity of cholesterol for cell membranes and its ability to change their properties, for example enhance their mechanical durability and decrease passive permeability (5–8). Also, cholesterol is an important component in the membranes of eukaryotic cells, and its homeostasis is critical to cell survival. Recent reports (9, 10) point to the importance of cholesterol in stabilizing membrane rafts containing receptors and describe the complex pathways for its biosynthesis, efflux, uptake, and trafficking. Very recently, a bioactive role for cholesterol has also been identified in the central nervous system, where its production by glial cells promotes improved synaptogenesis by surrounding neurons (11). We therefore thought that an anchoring biomaterial that could supply a universally fundamental molecule to mammalian cells would be an attractive substrate for cell attachment and proliferation.

Cholesterol was also selected because of the well known mesogenic nature of cholesterol and its derivatives, that is, their ability to self order into liquid crystalline substances (12, 13). Liquid crystalline matter was in fact discovered over a century ago by using cholesterol derivatives (12). As part of our system's design, oligoester chains of L-lactic acid and cholesterol are both considered to be easily biodegradable, thus making the system suitable for the preparation of tissue engineering templates that sustain cell proliferation and migration. Finally, higher molecular weight PLA is a common matrix material in tissue engineering scaffolds (14–19), and therefore the cocrystallization or secondary bonding of molecules studied here could easily occur on its surface. In this way, the self-assembling structures could be used to modify the internal surfaces of three-dimensional scaffolds fabricated from lactic acid or its copolymers with glycolic acid.

In this paper, we discuss the synthesis and characterization of various cholesteryl-(L-lactic acid) (C-LA) materials. The structural characterization has been carried out primarily through small-angle x-ray scattering (SAXS), optical microscopy, differential scanning calorimetry (DSC), transmission electron microscopy (TEM), electron diffraction, and atomic force microscopy (AFM). We then describe our initial studies on culturing of mouse fibroblasts on these novel biomaterials.

## Materials and Methods

**Synthesis and Sample Preparation.** The chemical structure of the family of molecules studied here is shown in Fig. 1. C-LA$_{\bar{n}}$ of different molar masses were synthesized by ring-opening polymerization of L-lactide at 70°C in toluene solutions (0.125 M) (20, 21). The polymerizations were initiated at room temperature by an aluminum alkoxide formed by the reaction of 1 equiv of triethylaluminum with 3 equiv of cholesterol [a more detailed description of these preparations can be found elsewhere (22)]. PLA was obtained from Medisorb ($M_r \approx 120{,}000$). Samples for x-ray diffraction experiments were solvent cast from 3 wt % solutions in methylene chloride on glass substrates. Single crystals were prepared for TEM analysis by dissolving the molecules in hot ethanol (0.1 or 0.05 wt %), then cooling these solutions to 25°C. A drop of this suspension was deposited on a copper grid covered with a carbon substrate and dried in air. Thin films for TEM were

This paper was submitted directly (Track II) to the PNAS office.

Abbreviations: PLA, poly(L-lactic acid); C-LA, cholesteryl-(L-lactic acid); SAXS, small-angle x-ray scattering; DSC, differential scanning calorimetry; TEM, transmission electron microscopy; AFM, atomic force microscopy; DHE, dehydroergosterol.

†To whom reprint requests should be addressed at: 2225 North Campus Drive, Northwestern University, Evanston, IL 60208. E-mail: s-stupp@northwestern.edu.

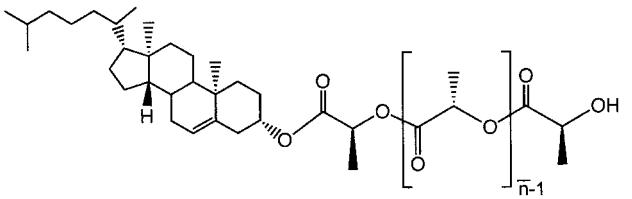


**Fig. 1.** Chemical structure of C-LA$_{\bar{n}}$.

prepared by casting 0.1 wt % solutions of these molecules in ethanol on carbon substrates at 80°C and subsequently cooling them to 25°C under a nitrogen atmosphere. Before TEM imaging, all samples were shadowed with Pt/C to enhance image contrast. Electron diffraction patterns were calibrated by using an Au standard evaporated directly on the samples.

**Methods.** Gel permeation chromatography was performed with Waters styragel HMW2 and styragel HMW 6E columns, 510 pumps, 486 UV detector, and 410 Refractive Index detector by using tetrahydrofuran as mobile phase. Polarized optical microscopy used a Leitz Laborlux 12POL optical microscope equipped with Linkam (Tadworth, U.K.) THM600 hot stage. Samples were kept under nitrogen atmosphere at elevated temperatures. SAXS experiments were carried out by using a Bruker (Billerica, MA) instrument with an Anton–Paar (Graz, Austria) high-resolution small angle camera, a Hi-Star (Bruker) Area Detector, a M18XHF22-SRA rotating anode generator, and Bruker software. Powder diffraction rings were integrated over 360° to yield the diffraction pattern by using a silver behenate calibration standard. The samples used for variable temperature studies were placed in sealed 0.7-mm-diameter capillary tubes. DSC experiments were performed by using a TA 2920 Modulated DSC instrument (TA Instruments, New Castle, DE) with a ramp speed of 10°C/min. TEM used a Phillips (Eindhoven, The Netherlands) CM12 instrument at 120 kV accelerating voltage. AFM images were acquired in tapping mode by using a Digital Instruments Multimode AFM and Nanoscope III controller, with 125-$\mu$m etched silicon probes. Typical forces were a few nanonewtons with scan rates of 0.5–1 Hz. Samples were prepared by casting films from 1 wt % solutions in methylene chloride on freshly cleaved mica surfaces.

**Cell Culture Experiments.** Glass Petri dishes used for cell culture experiments were specially prepared to have flat optically transparent bottom surfaces. The glass substrates were cleaned by first immersing them in a hot sulfuric acid bath for 10 min. The dishes were then rinsed thoroughly with water, purified by passage through a Milli-Q purification system (resistivity of 18.2 M$\Omega$·cm). Petri dishes were then placed in warm ammonium hydroxide/hydrogen peroxide mixture (4:1 by volume) for 10 min, then rinsed thoroughly with purified water and placed in HCl solution. Finally, dishes were rinsed extensively with water, dried with filtered nitrogen, and autoclaved at 126°C for 20 min before use. Substrates were prepared by solution casting films of the various materials under aseptic conditions. The materials were first dissolved in tetrahydrofuran at a concentration of 10 mg/ml and sterilized by passage through 0.22-$\mu$m filter membranes. Two milliliters of the solution was pipetted into each 2.7-cm-diameter Petri dish. Care was taken to be sure the solution was spread over the entire dish surface.

Substrates for quantitative cell studies were prepared on round glass coverslips, cleaned as described above. Each material was dissolved in tetrahydrofuran or $CHCl_3$ at 2 wt %. Coverslips were placed on a vacuum-chuck spincoater, and a few drops of the dissolved material (0.22 $\mu$m filtered) were added to the glass surface. The coverslips were spun at 1,500 rpm for 30 sec to obtain a thin uniform surface coverage (confirmed by profilometry) and were then placed in polystyrene multiwell plates for cell culture.

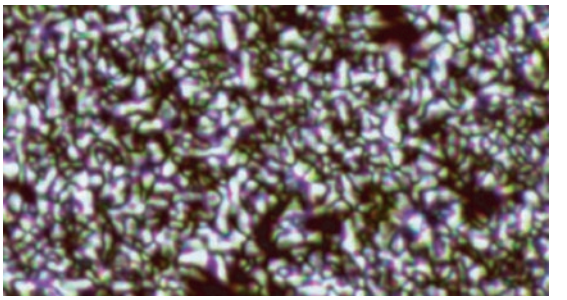

**Fig. 2.** Characteristic birefringent texture under crossed polars for C-LA$_{\overline{24}}$ at 25°C.

3T6 Swiss Albino mouse embryo fibroblasts (CCL-96, American Type Culture Collection) were cultured in DMEM supplemented with 10% (vol/vol) FBS and 1% penicillin–streptomycin. Cultures were incubated at 37°C in a humidified 5% $CO_2$ atmosphere, and the media were changed every 2 days. Subconfluent cells were dissociated with 0.25% trypsin and resuspended in culture medium. Cells were counted with a hemocytometer after trypan blue staining and seeded on the coated Petri dishes at a density of 10,000 cells/cm$^2$. 3T3 Swiss Albino mouse embryo fibroblasts (CCL-92, ATCC) were cultured in the same media and conditions as the 3T6 cells but in a 10% $CO_2$ atmosphere. FBS was obtained from HyClone Laboratories; all other cell culture media were from Invitrogen.

Optical microscopy analysis in cell culture experiments was carried out by using a Nikon TE200 instrument with phase contrast. Measurements of cell surface area were conducted by using NIH IMAGE and METAMORPH software. Between 7 and 25 measurements were taken for each substrate and timepoint. Data sets were analyzed by using ORIGIN software to determine statistical significance via ANOVA.

## Results and Discussion

C-LA$_{\bar{n}}$ ($\bar{n}$ = 8, 10, 11, 24, and 37) was synthesized in good yields (85–95%) with low polydispersities in the range of 1.05–1.15 as characterized by gel permeation chromatography. The characteristic birefringent texture for these materials at 25°C is shown in Fig. 2. This observation clearly indicates self-assembling behavior in these systems, and Table 1 shows the phase transitions observed by DSC. With increasing $\bar{n}$, both the glass transition and isotropization temperatures increase. The glass transition temperature for molecules with 10 lactic acid units is 32°C and increases to 49°C for 24 and 37 lactic acid units, respectively, still below the glass transition temperature for PLA, which is known to be ≈62°C. In addition, materials with longer lactic acid chains melt into a liquid crystalline phase at temperatures close to isotropization temperatures. For example, C-LA$_{\overline{37}}$ is liquid crystalline at 130°C and isotropic at 136°C. In contrast, Fig. 3 shows the DSC scan of C-LA$_{\overline{10}}$, revealing two well resolved endotherms at 57 and 88°C corresponding to a liquid-crystal-to-liquid-crystal transition and the isotropization transi-

**Table 1. Phase transitions observed by DSC**

| Material | $T_g$,* °C | $T_{s\text{-}s}$,† °C | Enthalpy, J/g‡ | $T_i$,§ °C | Enthalpy, J/g‡ |
|---|---|---|---|---|---|
| C-LA$_{\overline{10}}$ | 32 | 57 | 2 | 88 | 0.8 |
| C-LA$_{\overline{24}}$ | 49 | 128 | | 136 | 47 |
| C-LA$_{\overline{37}}$ | 49 | 130 | | 136 | 54 |

*$T_g$ = glass transition temperature; †$T_{s\text{-}s}$ = mesomorphic transition temperature between smectic phases; ‡$T_i$ = isotropization temperature; §The $T_{s\text{-}s}$ and $T_i$ transitions for C-LA$_{\overline{24}}$ and C-LA$_{\overline{37}}$ are resolved by DSC but are not separated. Therefore, the enthalpy numbers are estimated by peak resolution.

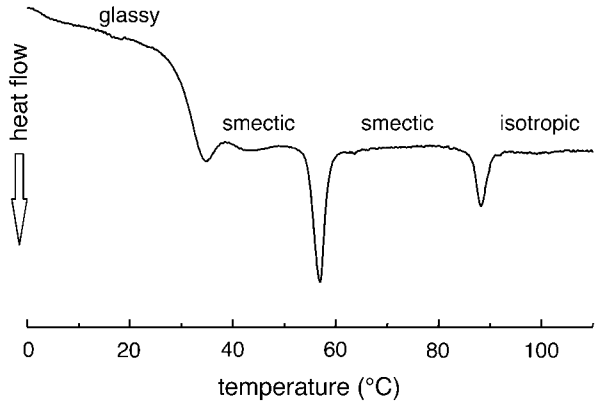


**Fig. 3.** DSC scan of C-LA$_{\overline{10}}$ revealing a glass transition at 32°C, a thermotropic liquid crystalline transition (smectic to smectic phase) at 57°C, and isotropization at 88°C.

tion, respectively. The enthalpy associated with the first endotherm is 2 J/g, suggesting this is a phase transition between two different smectic phases (23, 24).

Variable temperature SAXS scans before and after this first-order transition reveal (001) and (002) reflections, indicating lamellar organization of molecules in the materials and confirming their smectic nature (Fig. 12, which is published as supporting information on the PNAS web site, www.pnas.org). Above the glass transition temperature of 32°C, which is fully reversible in sequential DSC scans, this material is a thermotropic liquid crystalline substance. On the basis of optical microscopy between cross polars, order in this mesophase is retained below the glass transition temperature, as indicated by the retention of birefringence and the freezing of the fluid texture. Below $T_g$, the material can therefore be considered a liquid crystalline glass. No crystallization is observed on annealing at temperatures slightly above $T_g$, as is common in many crystallizable polymers. On the basis of data discussed above, we can conclude that C-LA$_{\overline{10}}$ exhibits a liquid crystalline state at body temperature (≈37°C). This fact indicates they could be used clinically as self-assembled fluids.

As stated before, SAXS scans of various samples reveal the formation of lamellar solids as indicated by (001) and (002) reflections (Fig. 4). The (001) reflections in Fig. 4 show periodicities of 58, 88, and 99 Å for C-LA$_{\overline{10}}$, C-LA$_{\overline{24}}$, and C-LA$_{\overline{37}}$, respectively. On the basis of molecular modeling [determined from molecular modeling (SYBYL) where the lactic acid units are in all trans conformation], the fully extended length of an average molecule with 10 lactic acid units is equal to 50 Å. If the oligo(L-lactic acid) chains are in a $10_3$ helical conformation, as observed in PLA crystals (26, 27), the length of a molecule with 10 lactic acid units would be equal to 43 Å. The cholesterol moiety measures approximately 15 Å, suggesting organization into a highly interdigitated bilayer. Fig. 4 *Inset* shows a model of interdigitated molecules demonstrating the observed d-spacing can be consistent with the proposed structure. Slight tilting of molecular axes relative to the layer normal may occur in these structures, as suggested by the small increase in d-spacing for systems with an average of 24 and 37 lactic acid units.

Fig. 5*a* shows a TEM and corresponding electron diffraction pattern of C-LA$_{\overline{37}}$ prepared by slow cooling of a hot ethanol solution. The micrograph reveals a characteristic morphology of stacked parallel layers that form a lozenge-shaped single crystal. Screw dislocations visible in the micrograph appear to play a key role in their formation. The electron diffraction pattern of the single crystal corresponds to an a*b* reciprocal lattice plane that can be indexed as an orthorhombic unit cell with lattice parameters a = 10.60 Å, and b = 6.00 Å. We also observed that PLA forms layered

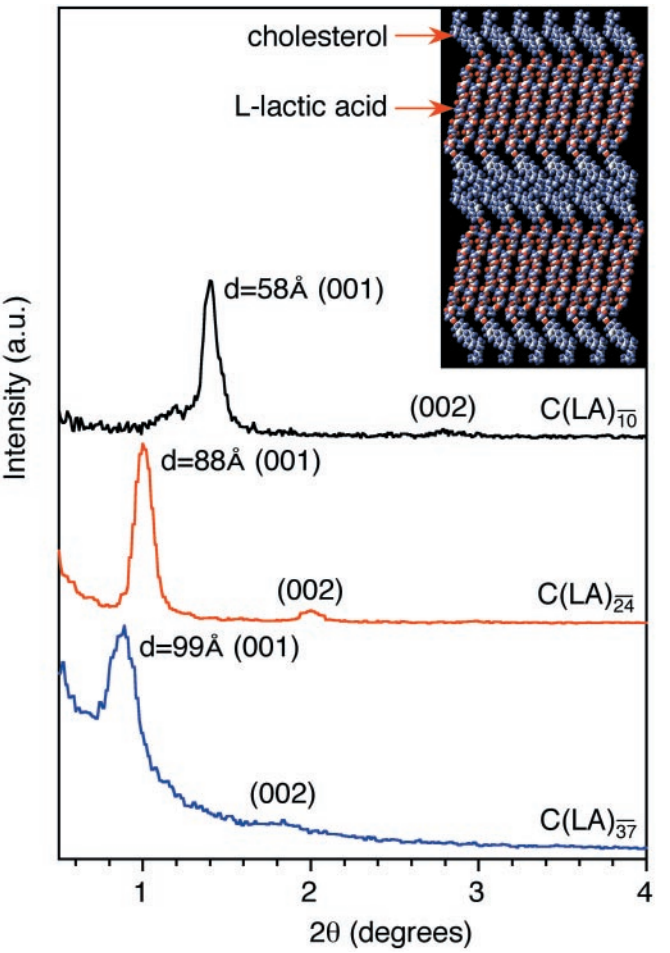


**Fig. 4.** SAXS scans of C-LA$_{\bar{n}}$ ($\bar{n}$ = 10, 24, 37), reveal (001) and (002) reflections indicating lamellar organization. (*Inset*) A molecular graphics model showing the proposed packing of C-LA$_{\overline{10}}$ molecules into a highly interdigitated bilayer with spacing of 58 Å. [Reproduced with permission from ref. 22 (Copyright 2002, Am. Chem. Soc.).]

single crystals (not shown) with an orthorhombic lattice, but its parameters are different from those observed in C-LAs. The lattice parameters for the polymer were a = 10.62 Å, and b = 6.04 Å, corresponding to the so-called $\alpha$ crystal, in which chains exist in a $10_3$ helical conformation (26, 27). By casting samples of cholesteryl derivatives of oligo(L-lactic acid) on carbon substrates from hot ethanol solutions and then cooling to room temperature, we were able to generate a different morphology consisting also of parallel stacked layers that are not organized into single crystals. This type of multilayer morphology is shown in Fig. 5*b*, revealing a film prepared from C-LA$_{\bar{8}}$. Fig. 5*b* also shows the a*b* electron diffraction pattern of the nonsingle crystal morphology revealing reflections distributed with hexagonal geometry that cannot be indexed as a hexagonal unit cell. Instead, the phase observed can be interpreted as three orthorhombic lattices with a = $\sqrt{b}$ rotated by 60° relative to each other about the molecular axis (the orthorhombic unit cell parameters of the smectic $E_h$ phase are a = 10.63 Å, b = 6.14 Å). Our laboratory previously described this phase as a smectic $E_h$ phase (28). If the same molecules are used to prepare a sample from room temperature solutions, single crystals are obtained with an orthorhombic unit cell with parameters a = 10.56 Å, and b = 6.12 Å (see Fig. 5*c*). All materials characterized here organize into stacked two-dimensional structures, because their *x*–*y* dimensions can be as large as 5 microns, and their characteristic period based on x-ray diffraction is only as large as 100 Å. The

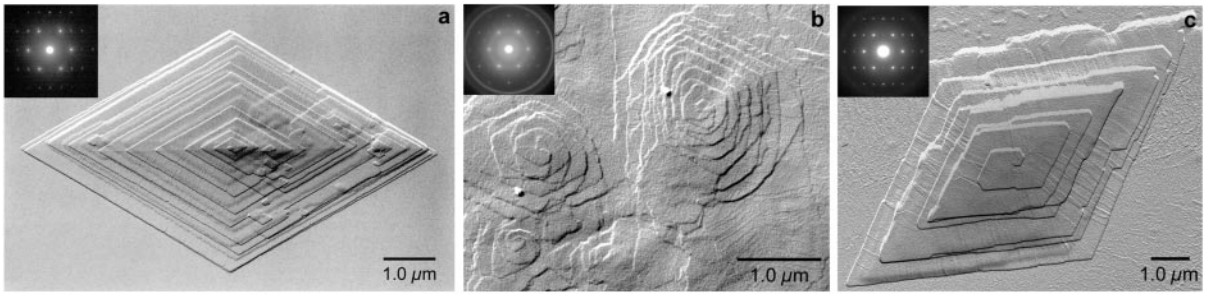


**Fig. 5.** (*a*) TEM image and electron diffraction pattern of single crystal C-LA$_{\overline{37}}$. (*b*) TEM image of a film of C-LA$_{\overline{8}}$ revealing multilayer domains formed by spiral dislocations. (*Inset*) Electron diffraction pattern (rings correspond to evaporated Au), indicating that the material is not a single crystal but a smectic $E_h$ liquid crystalline phase. (*c*) TEM image of a precipitate C-LA$_{\overline{8}}$ showing a multilayered lozenge-shaped single crystal formed by spiral dislocations. (*Inset*) Electron diffraction pattern revealing an orthorhombic unit cell.

biological significance of this architecture is that bioactivity in these biodegradable layers would be presented to cells many times as erosion reexposes periodically the same chemistry to cell surfaces. These biomaterials would be equivalent to stacks composed of multiple copies of a well defined monolayer and could be important as anchoring substrates for cells or even in drug delivery.

We studied the behavior of fibroblasts on substrates containing the multilayered structures. In our first experiments, we used 3T6 fibroblasts and observed qualitatively their response on solvent cast films of C-LA and PLA. Subsequently, we used 3T3 fibroblasts to obtain quantitative data, given the fact that these cells do not express rapidly extracellular proteins and are therefore more appropriate for studies of the effect of surfaces on cell behavior. The solvent cast films of C-LA$_{\overline{28}}$ used with 3T6 cells have a topography clearly visible by optical microscopy and AFM (Fig. 6). The ridges observed are characteristic of focal conic structures often observed in smectic liquid crystals (in this case, the ridges are 700 nm high and spaced about 8.5 $\mu$m apart). The behavior of 3T6 fibroblasts was studied 2 and 72 hr after cell seeding on surfaces of these materials. Cells were very loosely attached to surfaces of PLA, as shown by the round morphology in Fig. 7*a*. However, cells were firmly attached to one another when cultured on these specific surfaces. Entire colonies were easily dislodged from the culture surface as coherent sheets of cells, even when they were handled very gently.

PLA is a biocompatible and biodegradable synthetic polymeric material that has attracted great attention as a surgical repair material, e.g., for the development of synthetic vascular grafts (29–31) and medical sutures (32, 33) and as a temporary scaffold for cell growth in tissue-engineering applications (14, 15, 17–19). Generally, scaffolds fabricated from PLA, a hydrophobic polymer, have to be pretreated with ethanol to achieve cell spreading.

In great contrast, we found that cells adhered strongly to and spread well on solvent-cast films of the self-assembling material, C-LA$_{\overline{28}}$, which is a hydrophobic material as well (Fig. 7*b*). The adherent cells adopt a bipolar spindle shape, a fibroblastic morphology that is phenotypic for healthy cells in high-density cultures (34, 35). Once the surface is seeded, we observe confluency of the cells within 5 days. The surfaces presented to cells were prepared by using the method that yields the smectic $E_h$ phase as opposed to single crystal stacks discussed previously. We also observed erosion of material in locations where cells were previously attached. Interestingly, the observed adhesion and spreading of cells seem to occur on the surfaces of the domain boundaries of the focal conic ridges. We do not know why the ridges of the observed topography are avoided by cells relative to flat areas. However, other geometrical effects of this type have been described in the literature (36, 37).

Quantitative cell studies were conducted with 3T3 Swiss Albino mouse fibroblasts cultured on surfaces of C-LA$_{\overline{11}}$ (CL11), C-LA$_{\overline{24}}$ (CL24), PLA, PLA modified with CL24 (PLA-CL24), and ethanol-treated PLA (PLA-EtOH). The objective of these experiments was to quantify cell-surface adhesion, spreading, and proliferation. Films of the experimental materials were prepared by spin coating to yield smooth films and prevent formation of the ridges shown in Fig. 6. In this way, the interaction between cells and surfaces is dominated by surface chemistry and not by surface topography. Quantitative data on cell adhesion and spreading are reported in Table 2 and Fig. 8 and are discussed below.

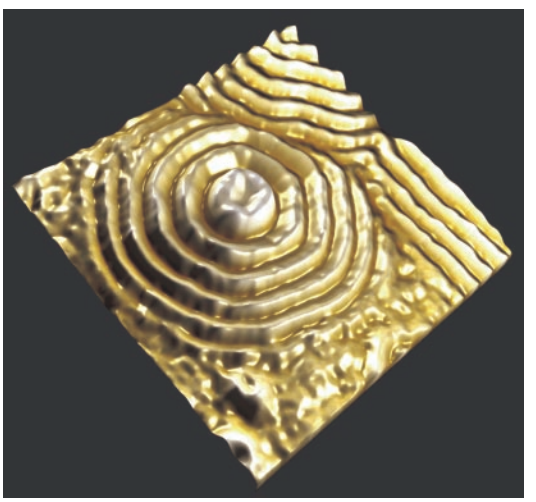

**Fig. 6.** AFM image showing the surface topography of C-LA$_{\overline{28}}$ films. The image is 106 × 106 microns.

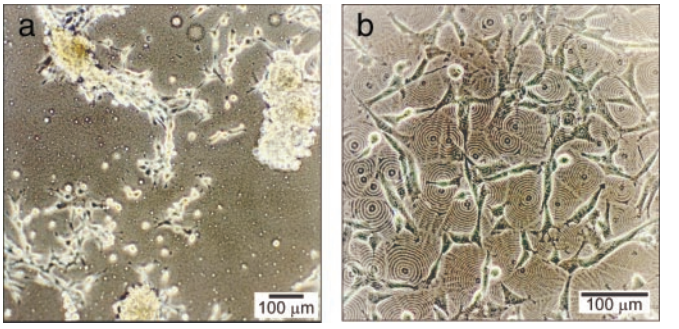


**Fig. 7.** (*a*) 3T6 fibroblasts on a PLA surface 72 hr after cell seeding. The fibroblasts aggregate and do not spread on these surfaces. (*b*) 3T6 fibroblasts on C-LA$_{\overline{28}}$ 72 hr after seeding. The cells spread preferentially along the boundaries of focal conic domains.

**Table 2. Percentage of total cells adhering to various biomaterials**

| Culture time | $CL_{\overline{11}}$ | $CL_{\overline{24}}$ | PLA-$CL_{\overline{24}}$ | PLA | PLA-EtOH |
|---|---|---|---|---|---|
| 2 hr | 54 | 58 | 61 | 41 | 43 |
| 1 day | 83 | 88 | 88 | 68 | 71 |
| 2 days | 86 | 86 | 90 | 88 | 80 |

Anchorage-dependent cells such as fibroblasts must adhere on surfaces to survive and proliferate (38, 39). This behavior is seen in both initial cell adhesion (i.e., the number of cells that adhere) and their sustained adhesion over time (i.e., for fibroblasts, the phenotypic increase in surface area over time). Table 2 shows the percentage of total cells that have adhered on various substrates after different time intervals in culture. Notably, after only 2 hr in culture, a higher percentage of cells is adhered on the surfaces of the self-assembling biomaterials studied here relative to PLA. In general, there is a substantial improvement in cell adhesion between 2 hr and 1 day in culture and only a nominal increase thereafter. After 2 days, over 80% of cells in culture have adhered onto these substrates, and this should be mediated by adhesive proteins synthesized by all cells regardless of substrate. The most important data in this table are the percentages of adhered cells after 2 hr in culture, because events that occur during the first few hours are critical for the survival and proliferation of cells. These results imply that modification of PLA surfaces with these self-assembling biomaterials promotes cell adhesion. It is known that the probability of cell survival, as well as the rate of proliferation, is greater when the rate of cell attachment is faster (37–41). The probability of success in tissue regeneration strategies should be closely coupled to the anchoring of cells to substrates during the first few hours of contact. This early behavior is critical for long-term formation of a viable and functional tissue, given that cell adhesion precedes tissue matrix synthesis. We therefore believe that multilayers that invite cell adhesion could be a valuable strategy for tissue engineering technologies.

The affinity of cells for a substrate can also be quantified by the average surface area of adherent cells over time. Fig. 8 shows the measured average surface areas of 3T3 fibroblasts on the various substrates over time.‡ Relative to PLA surfaces, substrates coated with molecular multilayers demonstrate a significant increase in cell spreading. For fibroblastic cells, this behavior is phenotypic and indicates an enhanced cell adhesion to the surface. The improvement seen in ethanol-treated PLA is expected and again represents a common strategy in *in vitro* experiments with PLA (43).

An additional observation of cell behavior on our materials is related to cell proliferation. We found that after 96 hr, PLA substrates modified by our self-assembling multilayers are populated by the highest number of adhered cells (Fig. 9). The observed increase of cell proliferation and spreading relative to that found on PLA suggests that a special bioactivity may be linked to these self-assembling materials. Whether this influence is because of altered adsorption of adhesion proteins, a more intrinsic effect of cholesteryl-based multilayers, or some other effect is still unknown at this time. In an effort to understand the observed effects, we present data below on cell uptake of the multilayers and on the interaction of cells with free cholesterol.

Given the importance of cholesterol homeostasis to mammalian cell survival, one should consider the potential role played by controlled release of cholesterol from our substrates as a result of layer-by-layer erosion of the multilayers. In this regard, we also have

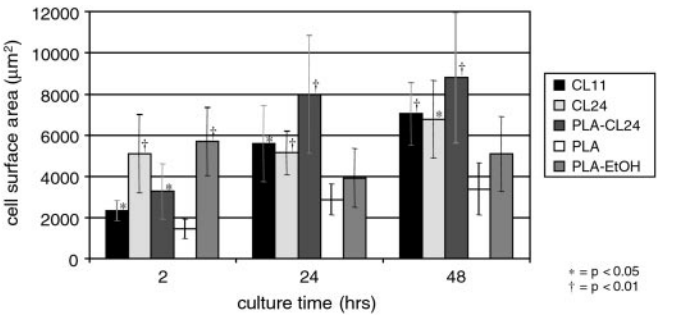


**Fig. 8.** Surface area of adhered cells on various biomaterials. Error bars are ± a 95% confidence level. All sample sets at each timepoint were compared by using ANOVA to the PLA control. *, $P < 0.05$; †, $P < 0.01$.‡

evidence that cholesterol moieties from the multilayered substrates are present in the cell membranes and within the cells. The experiment that led to this observation was carried out by using a fluorescent derivative of cholesterol, ergosta–5,7,9, (11), 22–tetraen-3$\beta$-ol, commonly referred to as dehydroergosterol (DHE) (Fig. 10). DHE is known to behave biologically as cholesterol (44, 45) but differs from cholesterol in that it has three additional double bonds and an extra methyl group.

We synthesized "DHE-(L-lactic acid)$_n$" (via a coupling route with a succinic anhydride linker) to yield a material that has very similar structure and properties to the other self-assembling materials prepared in this work. This material forms ordered multilayered structures just as the cholesterol-based molecules do (data not shown). However, the additional conjugation of DHE allows it to be visualized by fluorescence microscopy. DHE excites in the UV range and can be visualized with a standard Hg lamp and 4′,6-diamidino-2-phenylindole-range filter set. After 6 hr of exposure to DHE-LA, fibroblasts display intracellular and plasma membrane fluorescence characteristic of DHE (Fig. 11). Given that DHE is known to behave very similarly to cholesterol in other cell membrane experiments, this experiment supports our suggestion that cholesterol is indeed delivered to the cell from our materials.

The specific molecular design of the biomaterials studied here could be important in the observed cellular behavior. If delivery of cholesterol is fundamentally behind the enhanced bioactivity, one could suggest the simple mixture of PLA and cholesterol rather than synthesizing self-assembling diblock molecules of these two components. Yet, as verified in our laboratory, this mixture results in spontaneous-phase separation of PLA and cholesterol crystals and therefore fast dissolution of cholesterol crystals in media, posing the well-known problem of cytotoxicity induced by elevated levels of dissolved cholesterol (25). The self-assembled multilayers, on the other hand, offer the possibility of sustained controlled release of

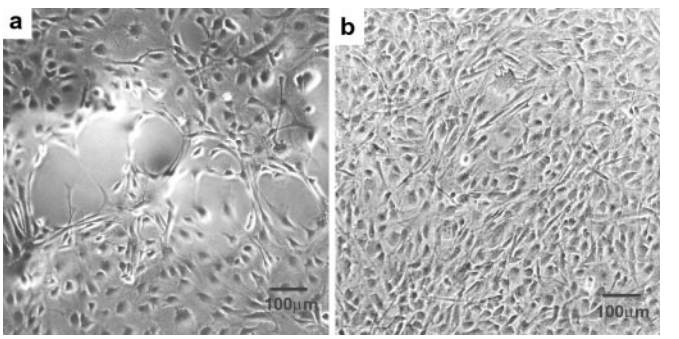


**Fig. 9.** 3T3 fibroblasts after 3 days of exposure to (*a*) a PLA surface and (*b*) a PLA surface modified with C-LA$_{\overline{24}}$. A higher population of cells is found on the surface in (*b*) modified with self-assembling multilayers.

‡The surface areas were determined by digitizing images of cells, tracing the perimeter of each cell by using either PHOTOSHOP or METAMORPH software and then NIH IMAGE or METAMORPH software for computation. Average surface area values for 3T3 cells on tissue culture polystyrene were: 1,400 $\mu m^2$ (2 hr), 4,400 $\mu m^2$ (24 hr), and 5,900 $\mu m^2$ (48 hr).

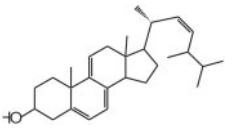

**Fig. 10.** Chemical structure of dehydroergosterol.

cholesterol for enhanced bioactivity (42). Given the ubiquity of cholesterol in mammalian cells, this strategy has potential for the regeneration of a variety of different tissues.

An additional advantage of our self-assembling system lies in its inherent ability to order as multiple layers of a material. This feature may yield a substantial benefit over other current PLA functionalization strategies, which are typically able to chemically modify only the outermost surface of PLA, producing only a single beneficial layer. Our system not only promotes initial cell adhesion but also repeatedly delivers a vital biological molecule to cells at the scaffold interface, with a consistent spatial orientation. Other ordered geometries in addition to multilayers may also be possible with modification of the basic C-LA design. It is clear from the observed biological response that cells interact with the cholesteryl-based self-assembling multilayers, and that enhanced proliferation and spreading are observed. However, this response could be due to a variety of intrinsic or nonspecific factors, the details of which are still uncertain.

Self-assembling biomaterials similar to the C-LA system could be potentially used on surfaces of porous three-dimensional tissue-engineering scaffolds. Periodic nanoscale multilayers could be coated onto the inner pore surfaces of scaffolds and then annealed through an appropriate temperature profile to freeze the ordered

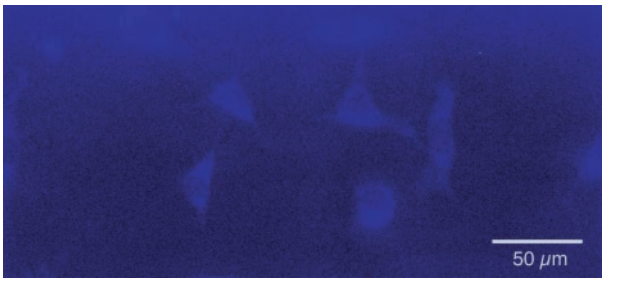


**Fig. 11.** 3T3 fibroblasts after 6 hr of exposure to a surface of DHE-(L-lactic acid)$_n$. Image was taken under epifluorescence illumination by using a 4′,6-diamidino-2-phenylindole-type filter set. The fluorescent material is visible throughout the cell cytoplasm and membrane.

phases. This is a strategy for repeated exposures of biologically relevant components to cells in a given location that would function effectively throughout a complex implant shape. Liquid crystalline phases would have more molecular mobility for binding interactions with cells, would chemically degrade faster, or would flow more easily to places where they are clinically needed. The systems described here demonstrate the potential of bulk self-assembly strategies for the design of biomaterials.

We are grateful to Janelle Gunther for obtaining the AFM images at the Visualization Laboratory of the Beckman Institute for Advanced Science and Technology. We acknowledge financial support from Boehringer Mannheim, the National Science Foundation (DMR9996253), and the Department of Energy (DEFG02–96ER45439). This work was partly carried out at the University of Illinois, Urbana–Champaign.



1. Whitesides, G. M., Mathias, J. P. & Seto, C. T. (1991) *Science* **254,** 1312–1319.
2. Lehn, J. M. (1995) *Supramolecular Chemistry* (VCH, New York).
3. Stupp, S. I., LeBonheur, V., Walker, K., Li, L. S., Huggins, K., Keser, M. & Amstutz, A. (1997) *Science* **276,** 384–389.
4. Kricheldorf, H. R. & Kreiser-Saunders, I. (1994) *Polymer* **35,** 4175–4180.
5. Dahl, J. S., Dahl, C. E. & Bloch, K. (1981) *J. Biol. Chem.* **256,** 87–91.
6. Dahl, J. S. & Dahl, C. E. (1983) *Proc. Natl. Acad. Sci. USA* **80,** 692–696.
7. Yeagle, P. L. (1985) *Biochim. Biophys. Acta* **822,** 267–287.
8. Yeagle, P. L. (1991) *Biochimie* **73,** 1303–1310.
9. Simons, K. & Ikonen, E. (2000) *Science* **290,** 1721–1726.
10. Simons, K. & Toomre, D. (2000) *Nat. Rev. Mol. Cell. Biol.* **1,** 31–39.
11. Mauch, D., Nägler, K., Schumacher, S., Göritz, C., Müller, E., Otto, A. & Pfrieger, F. (2001) *Science* **294,** 1354–1357.
12. Reinitzer, F. (1888) *Mh. Chem.* **9,** 421–441.
13. Lehmann, O. (1890) *Z. Kristallogr.* **18,** 464.
14. Vacanti, J. P., Morse, M. A., Salzman, W. M., Domb, A. J., Perez-Atayde, A. & Langer, R. (1988) *J. Pediatr. Surg.* **23,** 3–9.
15. Cima, L. G., Ingber, D. E., Vacanti, J. P. & Langer, R. (1991) *Biotechnol. Bioeng.* **38,** 145–158.
16. Freed, L. E., Vunjak-Novakovic, G., Biron, R. J., Eagles, D. B., Lesnoy, D. C., Barlow, S. K. & Langer, R. (1994) *Bio/Technology* **12,** 689–693.
17. Freed, L. E., Marquis, J. C., Nohria, A., Emmanual, J., Mikos, A. G. & Langer, R. (1993) *J. Biomed. Mater. Res.* **27,** 11–23.
18. Mooney, D. J. & Vacanti, J. P. (1993) *Transplant Rev.* **7,** 153–162.
19. Langer, R. & Vacanti, J. P. (1993) *Science* **260,** 920–926.
20. Löfgren, A., Albertsson, A.-C., Dubois, P. & Jérôme, R. (1995) *J. Macromol. Sci.–Rev. Macromol. Chem. Phys.* **C35,** 379–418.
21. Kricheldorf, H. R., Kreiser-Saunders, I., Jürgens, C. & Wolter, D. (1996) *Macromol. Symp.* **103,** 85–102.
22. Klok, H.-A., Hwang, J. J. & Stupp, S. I. (2002) *Macromolecules* **35,** 746–759.
23. Ginsburg, G. S., Atkinson, D. & Small, D. M. (1984) *Prog. Lipid. Res.* **23,** 135–167.
24. Vertogen, G. & deJeu, W. H. (1988) *Thermotropic Liquid Crystals, Fundamentals* (Springer, New York).
25. Tabas, I. (1997) *Trends Cardiovasc. Med.* **7,** 256–263.
26. Hoogsteen, W., Postema, A. R., Pennings, A. J., tenBrinke, G. & Zugenmaier, P. (1990) *Macromolecules* **23,** 634–642.
27. DeSantis, P. & Kovacs, A. J. (1968) *Biopolymers* **6,** 299–306.
28. Li, L. S., Hong, X. J. & Stupp, S. I. (1996) *Liquid Crystals* **21,** 469–483.
29. Niklason, L. E., Gao, J., Abbott, W. M., Hirschi, K. K., Houser, S., Marini, R. & Langer, R. (1999) *Science* **284,** 489–493.
30. Mooney, D. J., Mazzoni, C. L., Breuer, C., McNamara, K., Hern, D., Vacanti, J. P. & Langer, R. (1996) *Biomaterials* **17,** 115–124.
31. Zund, G., Hoerstrup, S. P., Schoeberlein, A., Lachat, M., Uhlschmid, G., Vogt, P. R. & Turina, M. (1998) *Eur. J. Cardio-Thorac.* **13,** 160–164.
32. Chu, C. C. (1982) *J. Biomed. Mater. Res.* **16,** 117–124.
33. Postlethwait, R. W. & Smith, B. M. (1975) *Surg. Gynecol. Obstet.* **140,** 377–380.
34. Vasiliev, J. M. & Gelfand, I. M. (1981) *Neoplastic and Normal Cells in Culture* (Cambridge Univ. Press, Cambridge, U.K.).
35. Kulonen, E. & Pikkarainen, J. (1973) *Biology of Fibroblast* (Academic, New York).
36. denBraber, E. T., deRuijter, J. E., Ginsel, L. A., vonRecum, A. F. & Jansen, J. A. (1996) *Biomaterials* **17,** 2037–2044.
37. Curtis, A. & Wilkinson, C. (1997) *Biomaterials* **18,** 1573–1583.
38. Ingber, D. E. (1990) *Proc. Natl. Acad. Sci. USA* **87,** 3579–3583.
39. Couchman, J. R., Rees, D. A., Green, M. R. & Smith, C. G. (1982) *J. Cell Biol.* **93,** 402–410.
40. Ruoslahti, E. & Reed, J. C. (1994) *Cell* **77,** 477–478.
41. Re, F., Zanetti, A., Sironi, M., Poletarutti, N., Lanfrancone, L., Dejana, E. & Colotta, F. (1994) *J. Cell Biol.* **127,** 537–546.
42. Gopalakrishna, P., Chaubey, S. K., Manogaran, P. S. & Pande, G. (2000) *J. Cell Biochem.* **77,** 517–528.
43. Mikos, A. G., Lyman, M. D., Freed, L. E. & Langer, R. (1994) *Biomaterials* **15,** 55–58.
44. Schroeder, F., Jefferson, J. R., Kier, A. B., Knittel, J., Scallen, T. J., Wood, W. G. & Hapala, I. (1991) *Proc. Soc. Exp. Biol. Med.* **196,** 235–252.
45. Schroeder, F., Woodford, J. K., Kavecansky, J., Woods, W. G. & Joiner, C. (1995) *Mol. Membr. Biol.* **12,** 113–119.